NUCLEAR ENGINEERING HANDBOOK

A collection of notes from the master of science in nuclear engineering

Pagliuca Simone
simone@pagliuca.net

Track: Nuclear Power Plants
Academic years: 2023∼2025

INTRODUCTION: lorem ipsum dolor sit amet, consectetur adipiscing elit. Donec auctor, nunc nec ultricies ultricies, nunc nunc.

Contents

I Experimental Reactor Kinetics

1 Control Rods

1.1 Introduction to Control Rods

1.1.1 Functions

Control rods are essential for **modulating reactivity**, serving the following functions:

- Compensating for excess reactivity due to fuel consumption or thermal feedback
- Regulating the neutron population
- Providing a safety margin for shutdown
- Assisting in reactor startup

1.1.2 Physical Behavior

Control rods function as **neutron absorbers** by altering the absorption component of K_{eff}:

$$K_{eff} = \frac{Production}{Absorption + Leakages} = \frac{\int\int \nu\Sigma_f \phi dV dE}{\int\int_{fuel} \Sigma_a \phi dV dE + \dot{L}} \tag{1.1}$$

1.1.3 Effects

The insertion of a control rod modifies the neutron flux distribution as shown in figure 1.1. Its effectiveness depends on its absorption capability and the neutron flux in its vicinity.

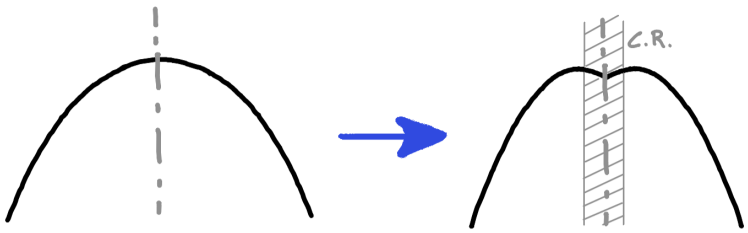

Figure 1.1: Flux before and after control rod insertion

Shadowing effect: The position of one control rod can impact the effectiveness of another.

1.1.4 Design

The **material** selection is critical, requiring a substance with high absorption capabilities. For example, B^{10} primarily undergoes (n,α) reactions, while Gadolinium is more likely to produce (n,γ) reactions, which raises radiological safety concerns.
Following material selection, the **rod geometry** is typically constrained by overall design parameters.
Finally, the required **number of rods**, or equivalently the pcm, is determined by the need to compensate for excess reactivity at the start of the fuel cycle and provide an adequate shutdown margin. This depends on the core design and technology. For istance the difference between the excess reactivity over time in a conventional burner reactor agaist a breeeder reactor (shown in fig. 1.2) shows the difference is needed reactivity compensation.

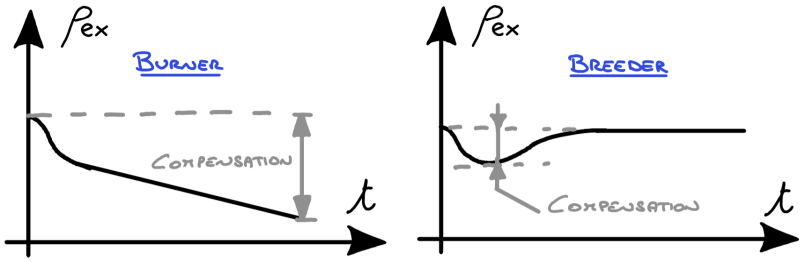

Figure 1.2: Reactivity worth needed for fuel consumption compensation is generally lower in breeder reactors compared to burner reactors.

1.1.5 Calibration

Calibration is necessary because the reactivity introduced by a control rod is not directly proportional to its insertion depth; instead, effectiveness varies with insertion depth, as illustrated in the following graphs:

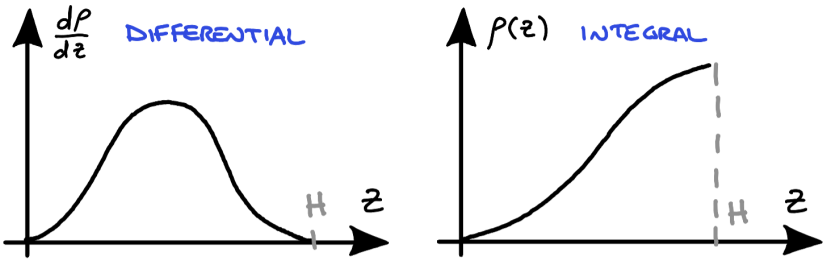

Figure 1.3: Differential and Integral reactivity curves

1.1.6 Formulas

The total reactivity worth ($\Delta\rho_{TOT}$) is given by:

$$\Delta\rho_{TOT} = \Delta\rho_{SM} + \Delta\rho_{EX} \tag{1.2}$$

where $\Delta\rho_{SM}$ is the shutdown margin and $\Delta\rho_{EX}$ is the reactivity excess.

Shutdown Margin:

$$\Delta\rho_{SM} = \rho_i(\text{Criticality}) - \rho_i(\text{Fully IN}) \tag{1.3}$$

Reactivity excess:

$$\Delta\rho_{EX} = \rho_i(\text{Fully OUT}) - \rho_i(\text{Criticality}) \tag{1.4}$$

1.2 Critical Calibration Method

1.2.1 Theory

The calibration of control rods in a reactor is crucial for understanding their reactivity worth. This can be accomplished using the in-hour and point kinetics equations to relate the time required to increase power by a factor to the reactivity.

Reactivity and Reactor Period

The relationship between reactivity (ρ) and the reactor period (T) is fundamental in control rod calibration. The point kinetics equations describe this relationship:

$$\frac{dP}{dt} = \frac{\rho - \beta}{\Lambda} P + \sum_{i=1}^{6} \lambda_i C_i \tag{1.5}$$

$$\frac{dC_i}{dt} = \frac{\beta_i}{\Lambda} P - \lambda_i C_i \tag{1.6}$$

where:

- P is the reactor power,
- ρ is the reactivity,
- β is the delayed neutron fraction,
- Λ is the prompt neutron lifetime,
- β_i and λ_i are the delayed neutron fractions and decay constants for each of the six precursor groups,
- C_i is the concentration of the i-th delayed neutron precursor group.

We can measure the reactor period T by inserting a control rod and observing the time required for the reactor power to increase by a factor e.
In practice we will use a factor 1.5 and compute the period as $T = \frac{\Delta t}{ln(1.5)}$.
We can then take advantage of the in-hour equation to correlate the reactivity to the reactor period:

$$\rho = \frac{\Lambda}{\mathbf{T}} + \sum_{i=1}^{6} \frac{\beta_i \lambda_i}{1 + \lambda_i \mathbf{T}} \tag{1.7}$$

We are going to use a 6 group apprach, the values of β_i and λ_i are known from montecarlo simulations and therefore come with their own uncertanty.

1.2.2 Pros and Cons of the Critical Method

Advantages:

- Absolute method: results are independent of other factors, including the position of other control rods
- High accuracy of results

Disadvantages:

- Time-intensive, as calibration is required for each control rod
- Reactor remains in supercritical condition during measurements

1.2.3 Experimental Procedure

Starting with a reactor in cold and clean conditions to avoid effects due to external poisons or thermal feedback.

1. Bring the reactor to a critical state.
2. Raise the REG rod by some steps
3. Measure the time required for the power to increase $3W \rightarrow 4.5W$.
4. Measure the time required for the power to increase $6W \rightarrow 9W$.
5. Adjust the shim rod to get back to criticality.
6. Repeat until the REG rod is fully withdrawn.

It is worth noting that the first measurment $3W \rightarrow 4.5W$ will take into also precursors, by the time of the second measurment most of them will be decayed so the measurment should be more rapresentative of the reactiviy.

1.3 Subcritical Control Rod Calibration

1.3.1 Introduction

The subcritical method provides an alternative approach to control rod calibration, particularly useful for cases where safety is a concern. This method allows for calibration while keeping the reactor in a subcritical state by using an external neutron source.

1.3.2 Theory - TBC

Subcritical Multiplication and Reactor Period

In subcritical conditions, the neutron population depends on both the external source and the reactor's multiplication factor K_{eff}. This dependency is described by the subcritical multiplication factor M:

$$M = \frac{1}{1 - K_{eff}} \tag{1.8}$$

With an external source, the neutron population evolves over generations until it reaches a steady state. This evolution can be described by a geometric series with K_{eff} as the ratio, where the number of generations required to reach steady state is:

$$N_{\text{steady}} \approx \frac{4}{\ln K} \tag{1.9}$$

Which means that the evolution is slower the closer we get to the steady state condition.

Point Kinetics Equations

To understand the reactor's response over time, we use the point kinetics equations adapted for the subcritical state:

$$\frac{dn}{dt} = K_{eff}\left(\frac{K_{eff} - 1}{K_{eff}} + \rho - \beta\right)\frac{n}{\Lambda} + \sum \lambda_i C_i + q \tag{1.10}$$

$$\frac{dC_i}{dt} = K_{eff}\frac{\beta_i}{\Lambda}n - \lambda_i C_i \tag{1.11}$$

where $\rho = \frac{\Lambda}{K}$ and q is the source term. The reactor period T is then given by:

$$T = \frac{1}{\lambda_1} \tag{1.12}$$

1.3.3 Experimental Procedure

The following steps outline the subcritical calibration procedure:

1. Bring the reactor in subcritical condition with all rods inserted.
2. Measure the neutron rate $\dot{R}$, we used a fission chamber, in pulse mode.

3. Insert the source and measure $\dot{R}$ again, we used $Ra\text{-}Be_r$.
4. Extract the control rods of which we know its reactivity worth and measure $\dot{R}$ once it reached steady state.
5. Compute the subcritical multiplication factor of the CR from known reactivity worth: $\Delta\rho = \rho_{out} - 0 = \frac{K-1}{K} \rightarrow M = \frac{1}{1-K}$.
6. Compute the calibration parameter $\alpha\Phi_s$ from this measurment: $\frac{\dot{R}}{M} = \alpha\Phi_s$.
7. Reinsert the control rod.
8. Extract another control rod and measure $\dot{R}$.
9. Compare measured $\dot{R}$ to the calibration parameter: $M = \alpha\Phi_s\dot{R}$
10. Repeat the last two steps for all control rods.

For better statistics take multiple measurements for each control rod (or long measurements).

Note on statistics: In poisson distributed data like radiation counts taking 20 short measurments each of time t will give the same statistical error as taking 1 longer measurement of time $T = 20t$.

1.3.4 Pros and Cons of the Subcritical Method

Advantages:

- Safe and keeps the reactor subcritical.
- Allows calibration of the shim, unlike other methods.

Disadvantages:

- Relys on the knowledge of one control rod's reactivity worth.
- Lower accuracy due to reliance on source and instrumentation.
- Only measures the total worth of the control rod, unable to get the full integral curve with reasonable measuring time (if we do a small step the variation in count rate change can easly hide in the noise and error).
- Frequent recalibration required due to burnup of fission chamber.

1.4 Definition

The reactivity coefficient, denoted as α, is defined as:

$$\alpha = \frac{\partial\rho}{\partial x} \tag{1.13}$$

where x represents a certain quantity that affects the reactivity, ρ.

1.5 Reactivity Coefficients for Different Components

For our case, we consider the following reactivity coefficients.

- α_f = Fuel reactivity coefficient
- α_m = Moderator reactivity coefficient
- α_c = Coolant reactivity coefficient
- α_e = Reactivity due to thermal expansion of the fuel

In the TRIGA reactor, α_e can often be neglected because, as in other thermal systems, the thermal expansion is smaller compared to the migration length of neutrons.

> **Note for fast reactors:** The higher migration length in fast reactors makes the reactivity effect of thermal expansion more relevant.

1.6 Doppler Effect

The fuel reactivity coefficient, α_f, is primarily due to the Doppler effect. The Doppler effect causes a broadening of the resonance peaks in the absorption cross-section of the fuel.

$$\sigma(\text{fuel, E}) = \text{Doppler Effect} \tag{1.14}$$

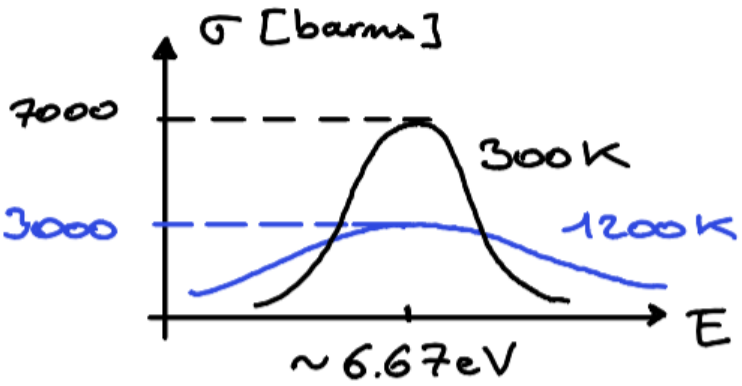

Figure 1.4: The Doppler effect shows the broadening of resonance peaks.

1.7 Functions of Reactivity Coefficients

Specifically for the TRIGA reactor:

- $\alpha < 0$ indicates a **negative reactivity coefficient**, which is essential for safety.
- $\alpha \ll 0$ allows for stable operation in *pulse mode*.

1.8 Design Considerations

When designing a system with fuel and moderator, consider the following:

- Increase in temperature ($T \uparrow$) leads to reduced moderation capability, affecting the neutron flux.
- The effect on the absorption cross-section ($\Sigma_a \downarrow$) also reduces the reactivity.

1.9 Physical Background

The physical background involves the following dynamics:

$$\frac{dn}{dt} = P - A - L + S \tag{1.15}$$

where:

- P denotes production, which depends on $\Sigma_f \phi$
- A denotes absorption, proportional to $\Sigma_a \phi$
- L denotes leakage, related to $\nabla D \phi$
- S denotes scattering, related to $\Sigma_s \phi$

The reactivity ρ can be approximated by:

$$\rho \propto \frac{P - A - L}{P} \tag{1.16}$$

1.9.1 Dependence on Parameters

The parameters affecting reactivity are:

- Temperature (affects cross-section and density)
- Geometry (affects distribution)
- Fuel condition (corrosion, burnup, etc.)

1.9.2 Side Note on Fast Reactors

In fast reactors, the coefficients α_f and α_c can be greater than zero depending on the fuel composition, as is the case with molten salt reactors where fuel is mixed with the coolant.

1.10 Overview of the Effects of Reactivity Coefficients

The following plot gives an overview of how reactivity feedbacks affect power in the reactor.

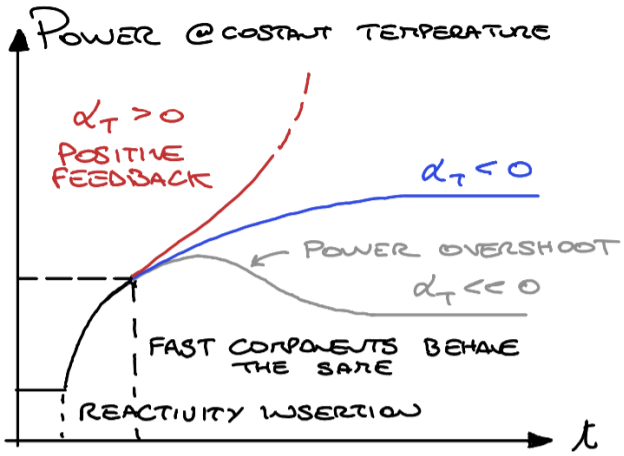

Figure 1.5: Overview of the effects of α on reactor power.

1.11 TRIGA Fuel

TRIGA fuel consists of Uranium-Zirconium Hydride (U-Zr-H), the solid moderator comprises hydrogen, with zirconium acting as the stabilizing element.

1.11.1 Experimental Findings

First Experiment: Mono-Energy Neutron Source

: Determination of the effective energy for moderation.

Second Experiment: Acoustical Resonance Study

: Influence of temperature on resonance peaks.

Third Experiment: Cross-Section Evaluation

: Measuring total removal cross-section.

1.12 Explanation of the Results

The findings from these experiments suggest that:

1. Hydrogen in a lattice has no free recoil.
2. The interference effect is characterized by a wavelength related to specific energy levels.
3. Possibility of up-scattering due to vibration modes.

1.13 Thermalization through Bounded Nuclei

The thermalization process occurs via two primary pathways:

1. **Translation Modes**:
   - Elastic interaction involving the entire crystal structure.
   - Reduced logarithmic energy decrease with increased temperature.
2. **Vibration Modes**:
   - Excitation of vibration states that influence up-scattering.
3. **Coherent and Incoherent Scattering**

The total scattering cross-section, $\sigma_{\text{scattering}}$, consists of both coherent and incoherent components:

$$\sigma_{\text{scattering}} = \sigma_{\text{coherent}} + \sigma_{\text{incoherent}} \tag{1.17}$$

In the TRIGA reactor

1.14 Elastic vs Inelastic Scattering

Elastic scattering involves no change in the internal quantum states of the scatterer. In contrast, inelastic scattering involves changes in these states.

- **Elastic**: No excitation states, such as with free hydrogen.
- **Inelastic**: Involves excitation related to vibrations and rotations within the molecule.

1.15 Thermalization through Bounded Nuclei

Thermalization of neutrons through bounded nuclei can occur via two primary mechanisms:

1. **Translation Modes**:
   - Elastic interactions that involve the entire crystal lattice.
   - Changes in temperature lead to variations in logarithmic energy decrease.
2. **Vibration Modes**:
   - Specific energy excitations related to vibrational modes.
   - Absorption of vibrational energy quanta can lead to up-scattering.

1.16 Coherent and Incoherent Scattering

Coherent scattering occurs when scattering events result in interference effects due to the crystal structure, manifesting as Bragg peaks. Incoherent scattering, in contrast, lacks such regular interference patterns.

$$\sigma_{\text{scattering}} = \sigma_{\text{coherent}} + \sigma_{\text{incoherent}} \tag{1.18}$$

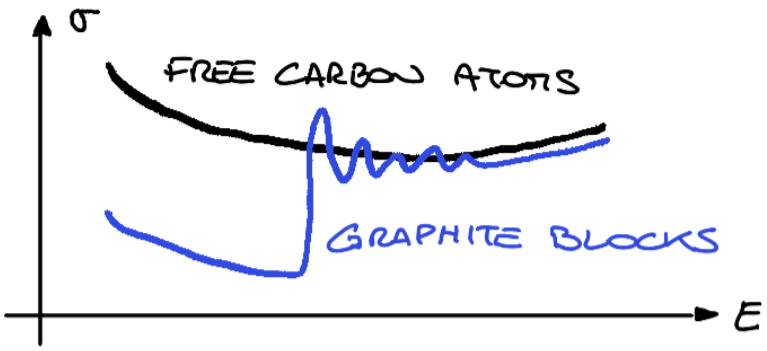

Figure 1.6: Coherent and incoherent scattering on Carbon atoms, when they form a crystalline structure in the graphite the scattering is inchoerent.

1.17 Summary of Findings on TRIGA Fuel

The experimental findings on TRIGA fuel reveal key insights into moderation and reactivity:

- TRIGA fuel demonstrates effective moderation properties above a certain energy threshold.

- The presence of zirconium hydride contributes significantly to the observed moderation effects.
- Doppler effects and up-scattering play important roles in spectral hardening.

1.18 Recap of Results

To summarize, the moderation capabilities of hydrogen in zirconium hydride are influenced by several factors, including lattice structure and vibrational modes. Based on experiments and Monte Carlo simulations:

- The Bragg peak is negligible in the energy range of interest.
- The primary mechanism involves vibrational modes related to the hydrogen lattice.
- Spectral hardening is observed with increasing temperature.

> The findings suggest that Zr-H-based fuels exhibit complex moderation behavior, particularly at higher temperatures where vibrational modes play a significant role.

1.19 Additional Notes

1.19.1 Composition of fuel reactiviy coefficent in the TRIGA reactor

A breakdown of the contributions to α_f in the TRIGA reactor is presented in the table below.

Contribution	Aluminum Cladding	Stainless Steel Cladding
Doppler Effect	2.6	2.1
Spectral Hardening	5.7	7.8
Cell Flux Effect	3.5	5.7
Leakage Effect	2.2	2.1
Total α_f (pcm/°C)	8.3	9.9

Table 1.1: Breakdown of α_f contributions in TRIGA for different cladding materials.

1.19.2 TRIGA Fuel Characteristics

TRIGA fuel (Zr-H) can moderate up to 0.13 eV and can induce upscattering, as indicated by experimental evidence, which justifies the use of H_2O as a moderator.

- Hydrogen is bounded to Zr, and for thermal energy, the bound cannot be neglected.

- Hydrogen in Zr-H moderates mainly through inelastic scattering.
- **Model:** Using the Einstein quantum harmonic oscillator, we can explain the experimental evidence.

In TRIGA fuel, the temperature coefficient α_T is approximately -7 to -9 pcm/°C.

1.20 Experimental Brief

- **Step 1:** Shift out control rods $\rightarrow \rho \uparrow \rightarrow$ Power $\uparrow$
- **Step 2:** Overshoot of power is observed.
- **Step 3:** Compute the energy release up to the peak.
- **Step 4:** Estimate the temperature T.
- **Step 5:** Compute the temperature coefficient α_T.

Note: The coolant temperature coefficient, $\alpha_{T_{\text{coolant}}}$, is slightly positive.

1.21 Void Coefficient

1.21.1 Definition and Function

The void coefficient, α_v, is defined as:

$$\alpha_v = \frac{\partial \rho}{\partial \mathcal{E}} \tag{1.19}$$

where $\mathcal{E}$ represents the void fraction. The void coefficient plays an important role in safety, helping assess the response in situations like boiling, experiments, irradiation, and Loss of Coolant Accidents (LOCA).

1.21.2 Design Considerations and Physical Background

- Changes in moderation due to void formation lead to spectral hardening, causing a decrease in the resonance escape probability p.
- Absorption decreases, increasing the thermal utilization factor f.
- Leakage increases, reducing the probability of non-leakage P_{NL}.

Figure 1.7: Effect of moderation ratio on k_{eff}.

1.22 Impact on the Six-Factor Formula

- p: Resonance escape probability

$$\alpha_{p,i} = \ln\left(\frac{1}{p}\right)\left(\frac{1}{N_H V_H}\frac{\partial N_H V_H}{\partial V}\right) = \frac{\partial p}{\partial V} \tag{1.20}$$

- f: Thermal utilization factor

$$\alpha_{f,i} = (1-f)\left(-\frac{1}{N_H V_H}\frac{\partial N_H V_H}{\partial V}\right) \tag{1.21}$$

These coefficients are strongly dependent on absorption and moderation capacity. For example:

- **Void in Fuel** $\rightarrow \rho\downarrow$
- **Void in Water** $\rightarrow \rho\uparrow$

1.23 Experiment Outline

1. Start at zero power, aiming to create a void.
2. Ensure zero power, clean, and critical conditions.
3. Register control rod positions.
4. Insert a sample filled with water:

- If $\alpha_v < 0$, $\rho \uparrow$

5. Return to criticality by adjusting the control rods.
6. Find control rod calibration curves to determine $\Delta\rho$.

Samples: Placed in one of the channels.

1.23.1 Examples of Void Experiments

- **In Ljubljana:** Bubbles were injected into the core. Monte Carlo simulations confirmed that $\alpha_v < 0$.
- **In Vienna:** Fuel elements with 70% enrichment were used, making $\alpha_v > 0$ due to high enrichment and the limited need for moderation.

1.24 Effects on Neutronics

The reactivity k can be expressed as:

$$k = \eta f \epsilon P_{NL} P_{NL} \tag{1.22}$$

The differential of k with respect to a parameter x_i can be expanded:

$$\alpha_i = \frac{\partial \rho}{\partial x_i} = \frac{1}{k}\frac{\partial k}{\partial x_i} = \frac{1}{\eta}\frac{\partial \eta}{\partial x_i} + \frac{1}{f}\frac{\partial f}{\partial x_i} + \frac{1}{\epsilon}\frac{\partial \epsilon}{\partial x_i} + \dots \tag{1.23}$$

- **Doppler Effect:** Variations in resonance weight due to self-shielding.
- **Spatial Self-Shielding:** Outer rings of the fuel pin shield the center, reducing the flux at the core.

1.25 Spectral Hardening

Spectral hardening occurs due to the harmonic oscillator behavior of Zr-H:

$$\alpha_{f,i} \approx \frac{1}{\Sigma_a^f}\frac{\partial \Sigma_a^f}{\partial x_i} - \frac{1}{\Sigma_a^m}\frac{\partial \Sigma_a^m}{\partial x_i} - \frac{1}{\phi}\frac{\partial \phi}{\partial x_i} \tag{1.24}$$

In fuel, spectral hardening increases the mean free path, affecting capture and escape probabilities.

1.25.1 Disadvantage Factor

$$\zeta = \frac{\phi_{\text{moderator}}}{\phi_{\text{fuel}}} \tag{1.25}$$

Since spectral hardening is stronger in the fuel, the ratio of escaping flux from the fuel is higher.

1.26 Experimental Procedure

This procedure yields a reactivity temperature coefficient rather than a prompt fuel coefficient.

- Measure ΔT due to $\Delta\rho$ and compute the ratio.
- No direct way to measure T_f (limited thermocouples, coolant contribution).

1.26.1 Simple Approach

1. Set reactor at desired power.
2. Record control rod position and extract positive reactivity.
3. Record power variation.
4. Calculate energy released until peak.
5. Calculate average temperature difference.

$$\Delta T_f = \frac{E}{G_f(N_f)} \tag{1.26}$$

6. Calculate the β temperature coefficient.

1.27 Coolant Effects

1.27.1 Components

Two contributions:

- Water density decrease, leading to $\rho \downarrow$
- Different rod capacity of H in water, leading to $\rho \uparrow$

Overall, $\alpha_{T_{\text{coolant}}} < 0$, although some contributions can be positive.

1.27.2 Isothermal Coefficient

$$\alpha_{\text{iso}} = \alpha_{T_f} + \alpha_{T_c} \tag{1.27}$$

Observed in Ljubljana by changing pool conditions while maintaining core conditions.

$$\alpha_{\text{iso}} = -3 + 6.5 = +3.5 \text{ pcm/°C} \tag{1.28}$$

Experimental Note: Despite positive contributions, $\alpha_{T_c} < 0$ overall.

2 Pulse Mode

2.1 Pulse Mode Operation

In pulse mode operation, the reactor is driven into a short, high-intensity power pulse. This mode is characterized by:

- Short duration
- High intensity

The observed parameters in pulse mode include:

1. Power (Intensity)
2. Time to reach peak power (to compare pulse duration)
3. Full Width at Half Maximum (FWHM) of the pulse

Figure 2.1: Illustration of pulse mode operation with parameters like peak power and FWHM.

2.2 Functions of Pulse Mode

Pulse mode can be used for various purposes, including:

- Activation analysis, including detector or semiconductor analysis
- Safety tests, such as reactivity insertion accidents
- Estimation of parameters related to reactor kinetics

2.3 Physical Background

In the pulse mode, the following sequence occurs:

$$\rho \uparrow\rightarrow P \uparrow\rightarrow E(T) \rightarrow T \uparrow\rightarrow \alpha_T \rightarrow \rho \downarrow\rightarrow \text{Feedback stabilizes the system.}$$

To translate energy into temperature, we need to know the heat capacity, C_p. The other important parameter is the temperature reactivity coefficient, α_f.

2.4 Experimental Evidence of Ljubljana Pulses

Videos of different reactivity insertions in the Ljubljana TRIGA reactor show that:

- Higher intensity in Cherenkov radiation correlates with larger $\Delta\rho$.
- Shorter pulses are achieved with larger $\Delta\rho$.
- The reactor is always scrammed after each pulse for safety, even if it is self-limited.

The Nordheim-Fuchs model is employed to understand the self-limited excursions during these pulses. The model incorporates several key assumptions:

1. Transients are modeled using point kinetics.
2. Delayed neutrons are neglected due to the short timescale.
3. The reactivity insertion, $\Delta\rho$, is treated as a step function.
4. Adiabatic heat transfer is assumed for the energy balance, focusing on the heat transfer to the coolant over a characteristic timescale.

The adiabatic assumption is valid only from a global perspective, as local variations in fission rates across individual fuel elements can lead to higher localized heat transfer coefficients (HTCs). This highlights the importance of understanding local phenomena in addition to the overall system behavior.

2.5 Nordheim–Fuchs Model

The Nordheim-Fuchs model is used to understand self-limited excursions over a short timespan. It relies on several assumptions:

1. Transient modeled with point kinetics
2. Delayed neutrons are neglected
3. $\Delta\rho$ is considered a step function
4. Adiabatic model for energy balance

Figure 2.2: Power pulse prediction by Nordheim-Fuchs model showing peak power and pulse duration.

2.5.1 Derivation of the Nordheim-Fuchs Model

The derivation of the Nordheim-Fuchs model begins with several simplifying assumptions:

1. Point kinetics approximation is used, ignoring spatial effects.
2. Delayed neutrons are neglected ($C_i = 0$) due to the short timescale of the pulse.
3. No external neutron source is present ($S = 0$).
4. Reactivity insertion, $\rho(t)$, is treated as a step function: $\rho(t) = \rho_0 H(t)$.
5. Heat transfer is modeled adiabatically, assuming no heat loss during the transient.

The rate of change of reactivity is given by:

$$\frac{dP}{dt} = \frac{\rho - \beta}{\Lambda} P,$$

where P is the power, β is the delayed neutron fraction, and Λ is the prompt neutron lifetime. For the temperature feedback:

$$\rho = \rho_0 - \alpha(T_f - T_{f,0}),$$

where α is the temperature reactivity coefficient and T_f is the fuel temperature. Using the adiabatic heat transfer model:

$$\frac{dT_f}{dt} = \frac{P}{m_f c_{p,f}},$$

where m_f is the fuel mass and $c_{p,f}$ is the specific heat capacity. Combining these equations leads to a coupled differential system that can be solved for $P(t)$ and $T_f(t)$.

After integration, the peak power and the Full Width at Half Maximum (FWHM) of the pulse can be derived:

$$P_{\text{max}} = \frac{m_f c_{p,f}}{\alpha} \left(\rho_0^2 - \beta^2\right),$$

$$\text{FWHM} = 3.52 \sqrt{\frac{\Lambda}{\alpha m_f c_{p,f}}}.$$

These expressions highlight the dependence of pulse characteristics on reactor parameters such as ρ_0, α, and m_f.

2.6 Power Pulse Parameters

The key parameters of a power pulse are:

- $\Delta\rho$: Known insertion value
- T_f: Fuel temperature from instrumentation
- E_{released}: Power integral for total energy release

2.7 Why TRIGA Can Operate in Pulse Mode

The TRIGA reactor can safely operate in pulse mode due to:

- Large prompt and negative temperature coefficient, $\alpha_f = -8$ to -10 pcm/K
- High heat capacity of the fuel-moderator combination

Note: In the Ljubljana TRIGA reactor, fewer control rods and elements with higher uranium content allow a unique pulse operation configuration.

2.8 Physical Phenomenon of the Pulse

The physical phenomenon during a pulse involves:

1. Large ρ insertion ($> 2\$$)
2. Prompt supercriticality reached
3. Fuel temperature increases, causing $\rho \downarrow$ until stability

Figure 2.3: Graph showing power pulse parameters and energy release.

2.9 Examples and Limitations

Examples of the results from the Nordheim-Fuchs model indicate:

- Increasing ρ_0 leads to higher peak power, reduced FWHM, increased energy in fuel, and larger ΔT_f.

Limitations of this model include:

- For slow pulses, delayed neutrons are no longer negligible, and their impact must be accounted for.
- The heat capacity, C_p, actually depends on the temperature, introducing non-linearities that the model does not capture.
- The model does not account for ramped reactivity insertions, assuming a step-like reactivity input instead.
- The point kinetics assumption ignores spatial effects, which may become significant in certain configurations.
- Experimental validation shows deviations in scenarios where local thermal feedback or hydrodynamic effects dominate.

2.10 Experimental Procedure

The following steps outline the experimental procedure for conducting pulse mode experiments:

1. Establish critical conditions with the transient rod inserted, then fully withdraw the transient rod to initiate the pulse.
2. Maintain the reactor at low power (approximately 1000 W) to avoid shadowing effects during the step insertion.
3. Fire the pulse by extracting the transient rod using the fast pneumatic system.
4. Scram the reactor approximately 15 seconds after the pulse to ensure safety.
5. Wait for the reactor to cool down before proceeding with further operations.

This chapter serves as a concise overview of key concepts in reactor dynamics and thermal-hydraulics that are foundational knowledge for further study and practical application. The material presented here is intended to recall principles, equations, and methodologies we are already familiar with, focusing on their relevance to reactor operation and safety analysis.

2.11 Dynamic Modeling

Dynamic modeling allows us to study power transients that are not feasible with Monte Carlo simulations. It plays a crucial role in:

- Safety analysis.
- Developing simulation tools for conceiving new experiments.

Dynamic modeling can be approached at different levels of complexity:

- Zero-dimensional (lumped parameter) models.
- One-dimensional (system code) models.
- Three-dimensional models using Computational Fluid Dynamics (CFD) coupled with diffusion/transport equations.

Verification and validation are essential:

- **Verification:** Ensuring the correctness of models and code implementation.
- **Validation:** Comparing model predictions with experimental data.

2.12 Zero-Dimensional Models

Zero-dimensional models focus on simplified interactions between core components, such as:

- **Reactivity:** Governed by control rod positions.
- **Neutronics:** Affecting power generation.
- **Thermal-Hydraulics:** Influencing coolant, fuel, and cladding temperatures.

These models provide a high-level understanding of reactor behavior under transient conditions by coupling these subsystems.

2.13 Thermal-Hydraulics

Thermal-hydraulic analysis examines heat transfer and fluid dynamics within the reactor. Key equations include:

- Energy conservation for the coolant.
- Momentum balance for natural convection or forced flow.
- Heat transfer correlations for cladding-to-coolant interfaces.

Examples and practical calculations illustrate typical parameter estimation, such as Reynolds and Nusselt numbers, and their impact on flow regimes and heat transfer efficiency.

2.14 Neutronics

Neutronics fundamentals are based on the point kinetics equations:

$$\begin{cases} \frac{d\psi}{dt} = \frac{\rho-\beta}{\Lambda}\psi + \sum_i \frac{\beta_i}{\Lambda}\gamma_i, \\ \frac{d\gamma_i}{dt} = \lambda_i(\psi - \gamma_i), \quad \forall i \text{ (delayed neutron precursor groups)}. \end{cases}$$

Here, ψ represents neutron density, γ_i are delayed neutron precursors, and ρ is reactivity.

Reactivity changes are expressed as:

$$\rho(t) = \alpha_f \Delta T_f + \alpha_c \Delta T_c + \alpha_m \Delta T_m$$

2.15 Advanced Considerations

Further refinements to models can include:

- Xenon, iodine, and samarium buildup.
- Inlet temperature variations and their effect on heat exchanger dynamics.

An example equation for the coolant pool when active cooling is operational:

$$m_{\text{pool}} c_p \frac{dT_{\text{pool}}}{dt} = \dot{m} c_p (T_{\text{out}} - T_{\text{pool}}) - \dot{m}_{\text{diffuser}} c_p (T_{\text{pool}} - T_{\text{diffuser}})$$

2.16 Thermal-Hydraulic Model: Overview

The thermal-hydraulic model represents the coupling between heat generation in the reactor core and the fluid flow used for cooling. It accounts for energy conservation, heat transfer, and fluid dynamics to ensure safe and efficient operation.

2.16.1 Energy Balance in Coolant

The energy conservation equation for the coolant is expressed as:

$$m_{\text{pool}} c_p \frac{dT_{\text{pool}}}{dt} = \dot{m} c_p (T_{\text{in}} - T_{\text{out}}) - \dot{Q}_{\text{loss}}$$

Where:

- m_{pool}: Coolant mass.
- c_p: Specific heat capacity of the coolant.
- T_{pool}: Average coolant temperature.
- $\dot{m}$: Mass flow rate.
- $T_{\text{in}}, T_{\text{out}}$: Inlet and outlet temperatures, respectively.
- $\dot{Q}_{\text{loss}}$: Heat losses due to various mechanisms like radiation and convection.

2.16.2 Natural Circulation

Natural circulation is modeled using momentum balance equations. It occurs due to density differences driven by temperature gradients in the reactor:

$$\Delta P_{\text{gravity}} = \Delta P_{\text{friction}} + \Delta P_{\text{form}}$$

Where:

- $\Delta P_{\text{gravity}}$: Pressure difference due to gravity.
- $\Delta P_{\text{friction}}$: Pressure drop due to pipe and channel friction.
- ΔP_{form}: Additional pressure drop due to form losses (e.g., bends, valves).

For a natural convection loop, the driving pressure is derived from buoyancy forces:

$$\Delta P_{\text{gravity}} = \rho g \Delta h$$

2.16.3 Heat Transfer Mechanisms

The heat transfer rate from the fuel to the coolant is governed by:

$$\dot{Q} = K(T_{\text{fuel}} - T_{\text{coolant}})$$

Where:

- $\dot{Q}$: Heat transfer rate.
- K: Overall heat transfer coefficient.
- T_{fuel}: Temperature of the fuel.
- T_{coolant}: Temperature of the coolant.

For subcooled nucleate boiling or forced convection, the Nusselt number (Nu) is used to correlate the heat transfer coefficient (h):

$$Nu = f(Re, Pr)$$

Where:

- Re: Reynolds number, indicating flow regime.
- Pr: Prandtl number, relating momentum and thermal diffusivity.

2.16.4 Practical Example

A worked example calculates key parameters for a simplified coolant system:

- **Mass flow rate** ($\dot{m}$):

  $$\dot{m} = \frac{\Delta P_{\text{driving}}}{\rho g h_f}$$

  Where h_f represents frictional head losses.

- **Reynolds number** (Re):

  $$Re = \frac{\rho v D}{\mu}$$

  Determines the flow regime (laminar or turbulent).

- **Heat transfer coefficient** (h):

  $$h = \frac{Nu \cdot k}{D_h}$$

  Where k is the thermal conductivity and D_h is the hydraulic diameter.

- **Critical heat flux (CHF)**: Critical to evaluate the boiling point and heat transfer capacity, ensuring safe operation.

2.16.5 System Dynamics

The coupled equations for temperature, flow, and pressure describe the dynamic behavior of the thermal-hydraulic system:

$$\begin{cases} \frac{dT_{\text{fuel}}}{dt} = \frac{1}{mc_p}\left(P_{\text{gen}} - \dot{Q}\right), \\ \frac{dT_{\text{coolant}}}{dt} = \frac{1}{\dot{m}c_p}\left(\dot{Q}_{\text{fuel-coolant}} - \dot{Q}_{\text{loss}}\right), \end{cases}$$

Where:

- P_{gen}: Power generated by fission reactions.

2.16.6 Natural Convection vs. Forced Circulation

Depending on the reactor design:

- **Natural convection** relies on buoyancy forces and is typically used in passive safety systems.
- **Forced circulation** employs pumps for higher flow rates, suitable for higher power reactors.

This section provides a concise recall of thermal-hydraulic principles, bridging fundamental equations and practical applications.

2.17 Focus on TRIGA Reactors

For TRIGA reactors, particular attention is given to:

- Limiting fuel temperature to prevent hydrogen production.
- Analyzing the central channel (highest power) and second channel (highest temperature).
- Assessing heat transfer modes, such as natural convection and subcooled nucleate boiling.

Heat transfer coefficients (α) are calculated using:

$$\alpha = \frac{\dot{m} \cdot k_{\text{cool}}}{D_h}$$

Different correlations may apply for various channels since there is no "common channel" in a triga reactor configuaration, and cross-flow effects are generally neglected. We should also check if we don't fall into subcooled boilin condition, the Bergles-Roshenow correlation is usually choosen.

Conclusion

This summary provides a structured recall of thermal-hydraulics principles, bridging fundamental equations and practical applications. These insights are crucial for both academic studies and real-world reactor operations.

2.18 Monte Carlo Analysis

In this chapter, we model an experiment conducted at the TRIGA reactor using the Monte Carlo code `Serpent` to compare results.

2.18.1 Comparison Between Deterministic and Stochastic Approaches

Deterministic methods provide exact solutions to approximated problems due to discretization. They are faster and allow for easy adjoint calculations. In contrast, stochastic methods, such as Monte Carlo, offer approximate solutions to exact problems. These methods are highly accurate but computationally expensive and make adjoint calculations difficult. Deterministic approaches are preferable for faster calculations, while Monte Carlo methods excel in accuracy for complex geometries.

2.18.2 Monte Carlo Method: Possible Approaches

The Monte Carlo method is particularly useful for solving problems involving complex geometries. The modeling approach depends on balancing accuracy and simplicity. The options include:

Point Kinetics: This is the simplest approach but provides the least accuracy. It assumes that the flux shape and energy spectrum remain constant. It is effective for simple transients and control experiments.

Diffusion Theory: Neglects angular dependence and uses a multi-group approximation. Cross-sections are averaged using:

$$\frac{1}{\phi}\int \Sigma d\Omega dE d\phi = \Sigma_{\text{group constants}} \tag{2.1}$$

However, it cannot neglect angle dependence in strongly absorbing materials, as this would lead to physically inconsistent results.

Transport Theory: The most accurate method, which requires discretizing space, energy, and angle in the integro-differential equations. It accounts for a wide range of unknowns and is essential for precise neutron tracking.

2.18.3 Pillars of the Monte Carlo Method

The Monte Carlo method is based on three fundamental pillars:

Transport: Tracks a neutron's journey from birth by fission to death by absorption or leakage.

Sampling: Accounts for potential interactions and their probabilities, ensuring accurate representation of physical processes.

Collection: Aggregates and interprets the simulated data to extract meaningful results.

2.18.4 Transport Pillar in Detail

In the Monte Carlo method, the transport process involves tracking a neutron's life cycle:

Initialization: Sample the neutron's initial energy and angle.

Free Path Sampling: Determine the distance to the next interaction site.

Collision Handling: Move the neutron to the collision site and sample the type of interaction:

- **Scattering:** Change the neutron's energy and angle and continue tracking.
- **Fission:** Record the number of neutrons produced, their positions, and continue tracking them.
- **Absorption:** Terminate the neutron's history.

Key questions during the transport process include:

- How to sample the free path?
- How to sample the interaction type?
- How to compute meaningful quantities from the simulation?

2.18.5 Sampling Pillar in Detail

The sampling process involves generating random variables to determine interaction points and outcomes:

The probability of no interaction up to a distance x is given by:

$$P_0(x) = e^{-\Sigma_{\text{tot}} x} \tag{2.2}$$

The cumulative density function (CDF) is used to sample the distance to interaction:

$$x = -\frac{1}{\Sigma_{\text{tot}}} \ln(\xi) \tag{2.3}$$

where $\xi \in (0, 1)$ is a random number.

Sampling methods include the **Inverse Method**, which involves the following steps:

1. Generate a random number $\xi \in (0, 1)$.
2. Find $\tilde{x}$ such that $F(\tilde{x}) = \xi$, where F is the cumulative distribution function.

For example, for $f(x) = \Sigma_T e^{-\Sigma_T x}$:

$$F^{-1}(\xi) = -\frac{1}{\Sigma_T} \ln(\xi) \tag{2.4}$$

If an interface between two materials is encountered, the following approaches can be used:

- **Adjust the Initial Sample:** Correct the initial sample to ensure conservation of probability. For example, if x_1 is the initial sampled position, adjust to x_2 based on the boundary location to maintain consistency.

$$e^{\Sigma_{tot}(x_1 - d) = e^{\Sigma_{tot}(x_2)}} \tag{2.5}$$

- **Sample Anew:** Use the information from crossing the boundary to take a new sample starting from the interface point x_2, ensuring accurate representation of the new region.

In both cases, the challenge lies in determining the distance to the interface and ensuring conservation of probability. Serpent uses *delta-tracking*: all the sampling is done with the same cross section: Σ_M called Majorant such that $\Sigma_m = \Sigma_{tot,i} + \Sigma_{virtual,i}$ We sample a virtual probability $P_{virtual} = \frac{\Sigma_{virtual}(i)}{\Sigma tot(i) + \Sigma_{virtual}(i)}$ from which we can get $P = 1 - \frac{\Sigma_{\text{region i}}}{\Sigma_m}$ which is the probability that the sampled point is virtual and should be rejected, if not, the point is valid.

Another sampling method involves **Sampling from Tables**, useful for cross-section data. This approach divides the range into N intervals such that:

$$\int_{x_1}^{x_2} f(x)dx = \frac{1}{N} \tag{2.6}$$

Ensuring equal probabilities across intervals allows direct sampling from cumulative tables. The sampled position can be refined using linear interpolation:

$$x = x_m + (N\xi - m)(x_{m+1} - x_m) \tag{2.7}$$

2.18.6 Collection Pillar in Detail

The collection process aggregates data from simulated neutron histories:

The sample mean $\bar{x}$ is calculated as:

$$\bar{x} = \frac{1}{N} \sum_{i=1}^{N} x_i \tag{2.8}$$

Variance is given by:

$$\text{Var}(\bar{x}) = \frac{\sigma^2}{N} \tag{2.9}$$

Confidence intervals are used to quantify uncertainty, typically expressed as:

$$\bar{x} \pm 2\sigma \tag{2.10}$$

Accurate results require a sufficient number of samples, as the standard deviation decreases with increasing N.

Uncertainty analysis is crucial for interpreting results, as demonstrated in cases like k_{eff} calculations:

$$k_{\text{eff}} = 1.0024 \pm 0.0002 \quad \text{(critical)} \tag{2.11}$$

2.19 Evaluation of $\beta_{\text{effective}}$ with Monte Carlo Codes

The delayed neutron fraction, β, plays a pivotal role in the kinetics of a nuclear reactor. Two primary distinctions of β are of interest: the physical delayed neutron fraction, β_{physical}, and the effective delayed neutron fraction, $\beta_{\text{effective}}$.

2.19.1 Physical and Effective Delayed Neutron Fractions

- **Physical Delayed Neutron Fraction** (β_{physical}): This represents the theoretical fraction of neutrons emitted by delayed neutron precursors and is determined from tabulated nuclear data. For the analyzed reactor system, $\beta_{\text{physical}} = 650$ pcm.
- **Effective Delayed Neutron Fraction** ($\beta_{\text{effective}}$): Unlike β_{physical}, $\beta_{\text{effective}}$ accounts for the neutron energy spectrum in the reactor. For the same reactor, $\beta_{\text{effective}} = 730$ pcm. This adjustment arises because delayed and prompt neutrons differ in their energy distributions. Delayed neutrons are more thermalized, necessitating a greater weighting factor to balance the spectral differences.

2.19.2 Mathematical Formulation of $\beta_{\text{effective}}$

The effective delayed neutron fraction can be evaluated using the following equation:

$$\beta_{\text{effective}} = \frac{\int_V \int_E \int_\Omega \Phi^*(\mathbf{r}, E, \Omega) \chi_d(E) \Sigma_f(\mathbf{r}, E) \Phi(\mathbf{r}, E, \Omega) \, d\mathbf{r} \, dE \, d\Omega}{\int_V \int_E \int_\Omega \Phi^*(\mathbf{r}, E, \Omega) \chi_t(E) \Sigma_f(\mathbf{r}, E) \Phi(\mathbf{r}, E, \Omega) \, d\mathbf{r} \, dE \, d\Omega}.$$

Here:

- $\Phi^*(\mathbf{r}, E, \Omega)$: Adjoint neutron flux.
- $\Phi(\mathbf{r}, E, \Omega)$: Forward neutron flux.
- $\chi_d(E)$: Energy spectrum of delayed neutrons.
- $\chi_t(E)$: Energy spectrum of all fission neutrons (prompt and delayed).
- $\Sigma_f(\mathbf{r}, E)$: Microscopic fission cross-section.

2.19.3 Importance in Monte Carlo Simulations

The adjoint flux Φ^*, which represents the importance of neutrons, is not directly available in standard Monte Carlo codes. To address this, the evaluation of $\beta_{\text{effective}}$ relies on alternative methods, such as:

- Weighting delayed neutron contributions by the relative thermalization of the neutron spectrum.
- Statistical sampling techniques to approximate the spectral weighting.

In Monte Carlo simulations, $\beta_{\text{effective}}$ can be approximated by:

$$\beta_{\text{effective}} \approx 1 - \frac{k_p}{k_{\text{eff}}}$$

where k_p represents the multiplication factor considering prompt neutrons only, and k_{eff} is the total effective multiplication factor including both prompt and delayed neutrons.

2.19.4 Physical Interpretation of the Results

The distinction between β_{physical} and $\beta_{\text{effective}}$ arises due to the spectral differences between prompt and delayed neutrons. Delayed neutrons, being closer to thermal energies, contribute more effectively to the chain reaction. Therefore, $\beta_{\text{effective}}$ provides a more accurate representation of the delayed neutron fraction in reactor dynamics.

2.20 Notes on Serpent Usage

Serpent is a 3D Monte Carlo code widely used for neutron transport and reactor physics calculations. Its capabilities include detailed modeling of geometry, materials, and reactor behavior, making it ideal for analyzing advanced nuclear systems.

2.20.1 Overview of Key Features

Serpent provides two estimates for the effective multiplication factor:

- **Analog** k_{eff}: Uses the direct statistical sampling of fission events.
- **Implicit** k_{eff}: Incorporates weighted contributions from neutron transport, reducing statistical uncertainty.

Both methods are valid and provide consistent results, but their use depends on the application and required level of accuracy.

2.20.2 Inputs for Serpent Simulations

To perform a simulation in Serpent, the following inputs are required:

1. **Nuclear Data Library**: Provides cross-section data for neutron interactions.
2. **Material Properties**: Includes isotopic compositions, densities, and temperatures of materials in the system.
3. **Geometry Definition**: The model must specify regions, cells, and boundaries. For instance:
    - Each material is assigned to a specific region.

- Universes are used to define the hierarchical structure of the model.
- A fuel element can be defined in a universe and replicated in a lattice.

4. **Population History**: Includes parameters such as:
   - Number of particles per cycle.
   - Number of active cycles (used in the final tally).
   - Number of inactive cycles (for initial flux convergence).
5. **Detector Setup**: Specifies the regions and reactions to monitor during the simulation. The response function R is defined as:

$$R = \int_V \int_E \int_\Omega \Phi(\mathbf{r}, E, \Omega) f(\mathbf{r}, E) \, d\mathbf{r} \, dE \, d\Omega,$$

   where f is the reaction rate or flux weighting function.

2.20.3 Analog vs Implicit Estimations

Serpent employs two approaches to calculate reaction rates:

- **Analog Estimation**: Directly counts the number of events, such as captures, fissions, and scatterings.
- **Implicit Estimation**: Uses statistical weights to account for multiple potential outcomes of a neutron's interaction. This method reduces uncertainty by including uncounted interactions through weighting.

For example, absorption can be represented as:

$$W = \prod \left(1 - \frac{\Sigma_{f,i}}{\Sigma_{t,i}}\right),$$

where W is the weight, $\Sigma_{f,i}$ is the fission cross-section, and $\Sigma_{t,i}$ is the total cross-section.

2.20.4 Practical Applications and Benefits

Serpent's hybrid use of analog and implicit methods allows users to:

- Reduce statistical uncertainty by increasing the number of points considered.
- Perform detailed analyses of complex geometries and materials.
- Simulate advanced reactor systems with high computational efficiency.

The implicit method is particularly advantageous for rare events, as it provides better statistical convergence without requiring additional computational cycles.

2.20.5 Considerations for Accuracy and Convergence

To ensure accurate results, users should:

- Define sufficient active and inactive cycles for flux stabilization.
- Verify that the detector response function is normalized correctly.
- Check that all material and geometry definitions align with physical system characteristics.

With these practices, Serpent can be a powerful tool for reactor physics research and design.